2D hexagonal boron nitride for solar energy conversions

A.A. Ramanathan
The University of Jordan, department of Physics, Amman-11942, Jordan

Abstract

The optoelectronic properties of free standing monolayer (ML) hexagonal boron nitride (h-BN) is investigated for potential solar energy conversion applications using the Density Functional Theory (DFT) full potential linearized augmented plane wave (FP-LAPW) method. In addition, the bulk optical properties have also been calculated for the sake of comparison. The dielectric functions, optical conductivities and the optical constants are evaluated using the relaxed structures from electronic total energy pseudopotential calculations. The results reinforce previous research on h-BN DUV optoelectronics and demonstrate the suitability of its use as a component in deep ultraviolet (DUV) and energy conversion devices.

Key words: DFT_PAW; DUV; dynamic electrical conductivity; dielectric function, optical constants

Introduction

The last two decades have seen tremendous research on two-dimensional (2D) materials similar to graphene; which was the first 2D material discovered with its honeycomb structure of single layer of carbon atoms with remarkable electronic, mechanical and optical properties [1-4]. Especially, layered transition metal dichalcogenides (TMDs) are widely investigated due to the rich diversity of properties which can be attributed to the finite and tuneable bandgap in these materials and have seen a multitude of applications [5-8].

In comparison to TMDs a less researched graphene analog is h-BN that is now gaining popularity as the key building block in van der Waal hetrostructures [9]. Similar to graphene 2D h-BN has a honeycomb structure but is insulating in character and consists of alternating B and N atoms that are sp^2 covalently bonded. However, due to difference in electronegativity of B and N atoms, the bond between B and N shows ionic character and is not purely covalent as in graphene. Being the structural analog of graphene h-BN is expected to possess and does show excellent mechanical properties and high chemical and thermal stabilities [10-12]. The small mismatch in lattice parameter of h-BN with graphene and the absence of dangling bonds and charge traps makes it an ideal substrate for graphene based devices [13, 14]. The indirect to direct bandgap crossover in MLs of TMDs with its efficient light matter coupling is also observed in h-BN [15, 16] and makes it a promising material for optoelectronics and deep ultraviolet (DUV) applications [17-19].

It is now the age of nano electronics and with the increasingly small size of components there is a need to extend optical systems to shorter wavelengths than visible light to improve the image resolution. This has motivated the interest in the short-wave UV region, especially DUV optics. The focus of the present study is to investigate the dynamic electrical conductivity and optical constants in order to better understand and substantiate previous research on h-BN DUV optoelectronics and its possible use as a component in solar energy conversion devices.

Calculation details

The calculations are carried out in two steps. First, DFT calculations using the ABINIT software program with the generalized gradient approximation (GGA) projector augmented wave (PAW) pseudopotentials [[20, 21]] are performed for structural optimization as in previous works [22, 23]. Convergence criteria of less than 1x10^{-6} Ha for the Self Consistent Field (SCF) iterations and force threshold of less than 1 mRy/a.u. for structural optimizations are used with the optimized k-point grid and cutoff energies for h-BN bulk and ML to obtain the relaxed structures and lattice constants.

Next, the relaxed geometries obtained are used to perform FP-LAPW calculations with the WIEN2k [24] code employing GGA_PBE to obtain the ground state energies and band structures. More stringent calculations using denser grids with a large number of k-points are used to evaluate the optical frequency dependent conductivities, real and imaginary parts of dielectric tensor, index of refraction, reflectivity, absorption and extinction coefficients.

Results

(a) Structural and electronic

Simulation of the 2D BN in the hexagonal structure is done by using the supercell technique. The optimized value of the bulk lattice constant is used to set up the super cell that contains a single atomic layer of h-BN separated by sufficient amount of vacuum in the z direction to offset any interactions between layers. The free standing h-BN ML is relaxed to obtain the ground state. The bulk and ML structures of h-BN are shown in Fig S1. The lattice constant values and band gaps for the optimized bulk and ML are listed in Table 1 and are consistent with those of other experimental and GGA-PBE calculations [16, 25-28]. The band structures of the bulk and ML h-BN are presented in Fig S2. We see an indirect K−M (bulk) to direct K−K band (ML) transition, consistent with recent results showing a direct wide bandgap value of 4.65 eV. This is also in accordance with other 2D materials like MoS_2 with indirect to direct band cross over from bulk to ML [8, 29]. In the past there was a controversy about the nature of the bandgap of h-BN bulk and ML, but with the recent experimental evidence using optical spectroscopy of Cassabois et al [15] and the work of Elias et al [16] who used a combination of deep-ultraviolet photoluminescence and reflectance spectroscopy with atomic force microscopy, it is now confirmed that there is an indirect to direct crossover in h-BN bulk to ML. The bandgap is much smaller than experiment in this work due to the well known problem of underestimation of GGA-DFT works.

Table 1 Structural and electronic properties of the relaxed h-BN

Compound	Space Group	Lattice constant (Å)		Bandgap (eV)		Interlayer spacing	Other works		
		a	c				a	c	bandgap
h-BN bulk	P63/mmc #194	2.517	6.706	4.23	K−M indirect	3.353	2.505^a 2.511^b	6.661^a 6.688^b	5.955^c
h-BN ML	P-6 m 2 #187	2.515	15.063	4.65	K−K direct	-			6.1^d

(a) Ref. 25 (b) Ref. 26 (c) Ref. 16, 27, 28 (d) Ref. 16

(b) Dynamical optical conductivities and constants

The term "optical conductivity" means the electrical conductivity in the presence of an alternating electric field or dynamic electrical conductivity. The term "optical" here implies the entire frequency range, and is not restricted to just the visible region. The imaginary part of the dielectric constant is related to the real part of the AC conductivity and, therefore, to the optical reflectivity and transmittance [30]. The real part of the dynamic electrical conductivity is connected with the energy absorbed by the electrons. The imaginary part of dielectric function, $\varepsilon_2(\omega)$, which represents absorption behavior, can be calculated from the electronic band structure. The real part of dielectric function, $\varepsilon_1(\omega)$, can be calculated according to Kramers-Kroing relation [31] which represents the electronic polarization under incident light. The optical conductivity and absorption behaviour of ML BN with respect to the photon energies are shown in Figure 1. We see from the figure the maximum conductivity and absorption peaks are at ~ 6, 11 and 13.5eV that is in the mid-UV and DUV regions considering the in-plane xx and perpendicular zz directions. There is also a small shoulder at around 4.5eV. We also note that both the xx and zz directions have almost similar magnitudes for the conductivity and absorption coefficients $\alpha(\omega)$. The absorption coefficient peak value is in good agreement with the experimental work of Li et al [32].

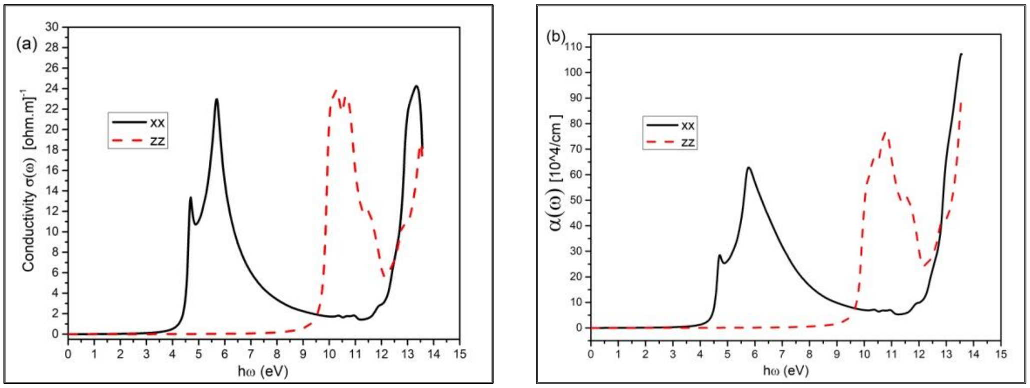

Figure 1. The optical conductivities and absorption coefficients for ML h-BN in the xx in-plane and zz out of plane directions.

A comparison with the supplementary information Figure S3 shows that the ML h-BN retains the bulk characteristics for the conductivities and absorption coefficients $\alpha(\omega)$, however, their magnitudes in the bulk are almost three times and two times more than the ML h-BN values respectively.

Figure 2 depicts the real and imaginary parts of the dielectric constant for the ML h-BN. The static values of the real dielectric constant are around 1.6 and 1.2 in the xx and zz directions respectively. Figs. 2(a) and (b) curves show the anisotropic behaviour in the two directions as in the previous conduction and absorption spectra Fig. 1.

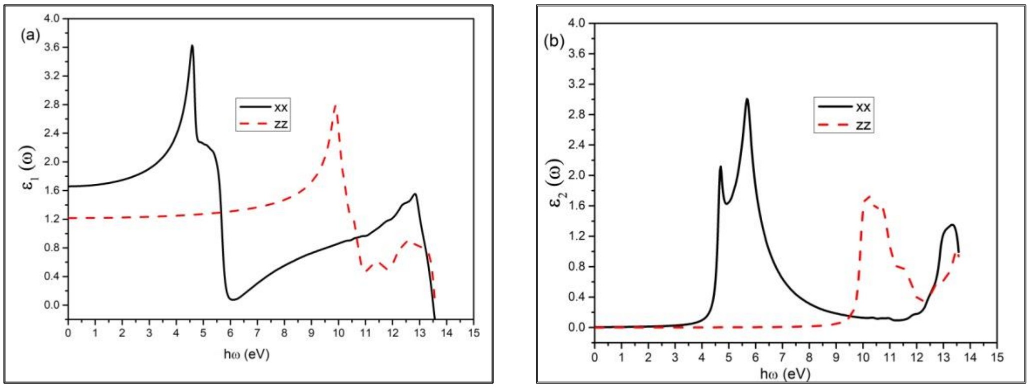

Figure 2. The real and imaginary parts of the dielectric function in the xx and zz directions for ML h-BN

However, for bulk h-BN, a look at Figure S4 shows that the static real dielectric constants are almost double in value around 3.6 and 2.3 in the in-plane and perpendicular directions respectively. A comparison of the magnitudes of the first sharp peaks of the imaginary dielectric constants Figs. 2(b) and S4(b) indicate the higher absorption capabilities of bulk as compared to that of ML h-BN.

From the values of $\varepsilon_1(\omega)$ and $\varepsilon_2(\omega)$ we can obtain the refractive index $n(\omega)$, reflectivity $R(\omega)$ and the extinction and absorption coefficients $k(\omega)$ and $\alpha(\omega)$ respectively from the relevant equations as detailed in the work [33]. The refractive index and extinction coefficients are shown in Fig 3. Once again we notice the anisotropy in the xx and zz directions. The static refractive index values obtained are 1.3 and 1.1 in the in-plane and of plane directions and ML h-BN is transparent in the IR and visible region for xx direction and also in mid-DUV for the zz direction as evinced from the flatness of the curves. A direct comparison of the refractive indices and extinction coefficients of the bulk and ML are depicted in S5 and S6. From S5 we see that the bulk values of $n(\omega)$ are consistently higher at 1.9 and 1.5 in the xx and zz directions and reflect the higher electron density in the bulk.

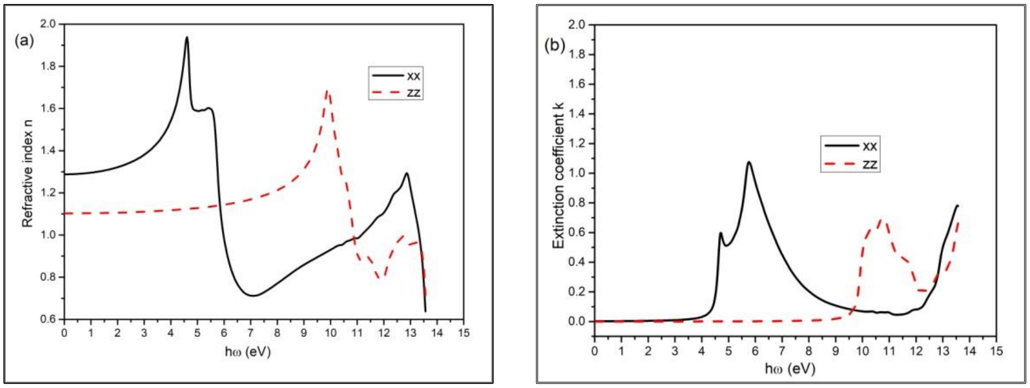

Figure 3. The refractive indices (a) and extinction coefficients (b) in the xx and zz directions for ML h-BN

The reflectivity plots for the ML and bulk h-BN are represented in Fig.4. The static values of reflectivity are very low both for ML and bulk h-BN and continues to be low over a wide range of photon energies 0-9eV for the perpendicular component which peaks in DUV region. Whereas, for the in-plane direction the reflectivity values are low in the visible and the first peak is around 6eV.

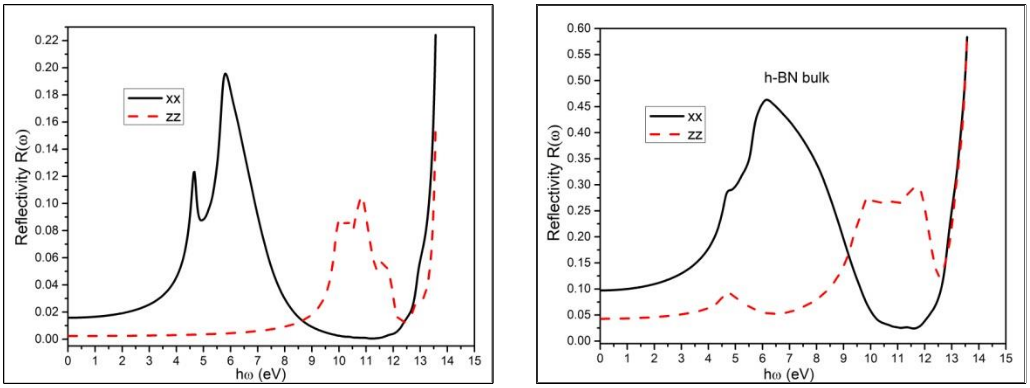

Figure 4. The reflectivity (a) for ML h-BN and (b) for bulk h-BN in the xx and zz directions

Discussion

The electronic structure calculations in this work confirms the previous literature results [15, 16, 27, 28] of the bandgap crossover of indirect to direct in h-BN bulk to ML. However, although the band gap values are in fair agreement with other theoretical works it is underestimated in comparison with experimental findings of 6.1eV in ML h-BN [16] due to the shortcomings of the GGA exchange correlation potential. A more accurate calculation using the Modified Becke-Johnson (mBJ) approximation [34, 35] is expected to give a better estimate for the bandgap and is part of future work.

The optical properties are qualitatively consistent with other theoretical and experimental works [16, 32, 36-38] and reinstate the importance of h-BN in DUV optoelectronics. Essentially the h-BN ML mimics the behaviour of the bulk and the shape and peak positions for the optical conductivity and constants are similar but the magnitude is much lower owing to the higher values of the dielectric constants in the bulk. Since, the attractive wide band and optical properties in DUV is maintained in the ML h-BN, with the added advantage of a direct bandgap, ML h-BN is a promising candidate for nano-optoelectronics in the DUV region. Numerous applications as DUV photo detectors/emitters, possible integration with graphene optoelectronics due its flatness and similarity in structure and close lattice constant values, and in addition its promise for realizing chip-scale DUV light sources are all waiting to be realized. Moreover, it can be argued that the optical properties of h-BN in the ultraviolet are very useful for the study of peptides and other biomolecules [16, 39, 40].

Supplementary Information: https://doi.org/10.6084/m9.figshare.17708465.v2

References

1. Max C. Lemme, "Current Status of Graphene Transistors", Solid State Phenomena, 156-158, Pages 499-509, 2010.
2. Garnica B, S. A., Knaust, M., & Fatikow, S. (2019). Automatic Micro-Robotic Identification and Electrical Characterization of Graphene. *Micromachines*, *10*(12), 870.
3. Aqra M.W. and Ramanathan A.A. Graphene and related 2D materials for desalination: A review of recent patents. *Jordan J. Phys.* 2020, *13 (3)* 233-242
4. Szunerits, S., and Boukherroub, R. Graphene-based biosensors. *Interface Focus* 2018 8:20160132. doi: 10.1098/rsfs.2016.0132
5. Ramanathan AA and Khalifeh JM (2018). Enhanced thermoelectric properties of suspended mono and bilayer of MoS_2 from first principles. IEEE Transactions on nanotechnology, 17(5), 974
6. Chen, Y.; Tan, C.; Zhang, H.; Wang, L. Two-Dimensional Graphene Analogues for Biomedical Applications. *Chem. Soc. Rev.* 2015.
7. D. Vikraman, K. Akbar, S. Hussain, G. Yoo, J-Y. Jang, S-H. Chun, J. Jung, H.J. Park: Direct synthesis of thickness-tunable MoS_2 quantum dot thin layers: Optical, structural and electrical properties and their application to hydrogen evolution. *Nano Energy*, **35**, 101 (2017).
8. Ramanathan AA and Khalifeh JM (2021). Thermoelectrics of $MoS_{2(1-x)}N_{2x}$ compounds. DOI: 10.23880/psbj-16000167
9. Geim, A. K. & Grigorieva, I. V. Van der Waals heterostructures. Nature 499, 419–425 (2013).
10. Zhi, C. Y.; Bando, Y. ; Tang, C. C.; Kuwahara, H.; Golberg, D. Large-scale fabrication of boron nitride nanosheets and their utilization in polymeric composites with improved thermal and mechanical properties. Adv. Mater. 2009, 21, 2889.
11. Grosjean, B., Pean, C., Siria, A., Bocquet, L., Vuilleumier, R., & Bocquet, M. L. (2016). Chemisorption of Hydroxide on 2D Materials from DFT Calculations: Graphene versus Hexagonal Boron Nitride. *The journal of physical chemistry letters*, *7*(22), 4695–4700.

12. Ramanathan AA., Aqra MW and Al-Rawajfeh AE Recent advances in 2D- nanopores for desalination. ECLE 2018, 16(4) 1217-1231.
13. Wang, M., Jang, S. K., Jang, W. J., Kim, M., Park, S. Y., Kim, S. W., Kahng, S. J., Choi, J. Y., Ruoff, R. S., Song, Y. J., & Lee, S. (2013). A platform for large-scale graphene electronics--CVD growth of single-layer graphene on CVD-grown hexagonal boron nitride. Advanced materials, *25*(19), 2746–2752.
14. Khan, A., Islam, S. M., Ahmed, S., Kumar, R. R., Habib, M. R., Huang, K., Hu, M., Yu, X., & Yang, D. (2018). Direct CVD Growth of Graphene on Technologically Important Dielectric and Semiconducting Substrates. Advanced science, *5*(11), 1800050.
15. Cassabois, G., Valvin, P. & Gil, B. Hexagonal boron nitride is an indirect bandgap semiconductor. Nat. Photon. 10, 262–266 (2016)
16. Elias, C., Valvin, P., Pelini, T. *et al.* Direct band-gap crossover in epitaxial monolayer boron nitride. Nat Commun 10, 2639 (2019).
17. Watanabe, K., Taniguchi, T. & Kanda, H. Direct-bandgap properties and evidence for ultraviolet lasing of hexagonal boron nitride single crystal. Nat. Mater. 3, 404–409 (2004).
18. Liu, H., Meng, J., Zhang, X., Chen, Y., Yin, Z., Wang, D., Wang, Y., You, J., Gao, M., & Jin, P. (2018). High-performance deep ultraviolet photodetectors based on few-layer hexagonal boron nitride. *Nanoscale*, *10*(12), 5559–5565.
19. Yin, J., Li, J., Hang, Y., Yu, J., Tai, G., Li, X., Zhang, Z. and Guo, W. (2016), Boron Nitride Nanostructures: Fabrication, Functionalization and Applications. Small, 12: 2942-2968.
20. A. A. Ramanathan. A DFT calculation of Nb and Ta (001) Surface Properties, JMP_ Special issue-DFT 2013, *4*, 432-437.

21. Torrent, F. Jollet, F. Bottin, G. Zerah, and X. Gonze Implementation of the Projector Augmented-Wave Method in the ABINIT code. M Comput. Mat. Science 42, 337, (2008).
22. A.A. Ramanathan and J.M Khalifeh (2017). Substrate matters: Magnetic tuning of the Fe monolayer. JMMM 426, 450-453.
23. Ramanathan A.A., Khalifeh J.M, Hamad B (2008) Evidence of surface magnetism in the V/Nb(0 0 1) system: A total energy pseudopotential calculation. Surf. Sci., 602, Issue 2, 607-613.
24. P. Blaha, K.Schwarz, F. Tran, R. Laskowski, G.K.H. Madsen and L.D. Marks, J. Chem. Phys. (2020) 152, 074101
25. R. W. Lynch, H. G. Deickamer, Effect of High Pressure on the lattice Paramers of Diamond, Graphite, and Hexagonal Boron Nitride. J. Chem. Phys. 44(1), 181–184 (1966).

26. Bin Xu, Meizhe Lv, Xiaohong Fan, Wen Zhang, Yong Xu & Tongguang Zhai (2015) Lattice Parameters of Hexagonal and Cubic Boron Nitrides at High Temperature and High Pressure. Integrated Ferroelectrics, 162:1, 85-93
27. Vuong, T. Q. P. et al. (2017) Phonon symmetries in hexagonal boron nitride probed by incoherent light emission. 2D Mater. 4, 11004
28. Schuster, R., Habenicht, C., Ahmad, M., Knupfer, M. & Büchner (2018) B. Direct observation of the lowest indirect exciton state in the bulk of hexagonal boron nitride. Phys. Rev. B 97, 041201
29. Mak, K. F.; Lee, C.; Hone, J.; Shan, J.; Heinz, T. F. Atomically thin MoS2: A new direct-gap semiconductor. Phys. Rev. Lett. 2010, 105, 136805.
30. Ashcroft, N.W. and Mermin, N.D. (1976) Solid State Physics, Saunders College Publishing.
31. Kramers H A 1927 Atti del Congresso Internazionale dei Fisici vol 2 (Bologna: Zanichelli) p 545; Kronig R de L 1926 J. Opt. Soc. Am. 12 547
32. Li J, Majety S, Dahal R, Zhao WP, Lin JY, Jiang HX. Dielectric strength, optical absorption, and deep ultraviolet detectors of hexagonal boron nitride epilayers. Appl Phys Lett 2012;101:67–92.
33. Ramanathan A.A.; Khalifeh J.M. Electronic, magnetic and optical properties of XScO3 (X=Mo, W) perovskites *PeerJ Materials Science* 3:e15 https://doi.org/10.7717/peerj-matsci.15
34. F. Tran, P. Blaha, Accurate band gaps of semiconductors and insulators with a semilocal exchange-correlation potential, Phys. Rev. Lett. 102 (2009) 226401.
35. Ramanathan, A.A. First Principles Investigation of the Optoelectronic Properties of Molybdenum Dinitride for Optical Sensing Applications. *Chem. Proc.* 2021, *5*, 27.
36. R. Gao, L. Yin, C. Wang, Y. Qi, N. Lun, L. Zhang, Y. X. Liu, L. Kang and X. Wang, J. Phys. Chem. C, 2009, 113, 15160– 15165.
37. Wang J, Cao S, Sun P, Ding Y, Li Y, Ma F. Optical advantages of graphene on the boron nitride in visible and SW-NIR regions. RSC Adv 2016;6:111345–9.
38. Wang, J., Ma, F., & Sun, M. (2017). Graphene, hexagonal boron nitride, and their heterostructures: properties and applications. *RSC Advances, 7*, 16801-16822.
39. Ferreira F, Chaves A J, Peres N M R and Ribeiro R M 2019 Excitons in hexagonal boron nitride single-layer: a new platform for polaritonics in the ultraviolet J. Opt. Soc. Am. 36 674
40. Henriques JCG, Ventura GB, Fernandes CDM and Peres NMR. Optical absorption of single-layer hexagonal boron nitride in the ultraviolet. J. Phys.: Condens. Matter 32 (2020) 025304